

# Classical and quantum fold catastrophe in the presence of axial symmetry

G. Dhont\* and B. I. Zhilinskiĭ

*Université du Littoral Côte d'Opale, Laboratoire de Physico-Chimie de l'Atmosphère,  
UMR 8101 du CNRS, 189A avenue Maurice Schumann, 59140 Dunkerque, France*

(Dated: September 5, 2008)

We introduce a family of Hamiltonians with two degrees of freedom, axial symmetry and complete integrability. The potential function depends on coordinates and one control parameter. A fold catastrophe typically occurs in such a family of potentials and its consequences on the global dynamics are investigated through the energy-momentum map which defines the singular fibration of the four-dimensional phase space. The two inequivalent local canonical forms of the catastrophe are presented: the first case corresponds to the appearance of a second sheet in the image of the energy-momentum map while the second case is associated to the breaking of an already existing second sheet. A special effort is placed on the description of the singularities. In particular, the existence of cuspidal tori is related to a second order contact point between the energy level set and the reduced phase space. The quantum mechanical aspects of the changes induced by the fold catastrophe are investigated with the quantum eigenstates computed for an octic potential and are interpreted through the quantum-classical correspondence. We note that the singularity exposed in this paper is not an obstruction to a global definition of action-angle variables.

PACS numbers: 45.20.Jj Lagrangian and Hamiltonian mechanics; 33.20.Tp Vibrational analysis  
Keywords: Fold catastrophe, Integrable Hamiltonian, Action-angle variables, Monodromy

## I. INTRODUCTION

Quantum mechanics is the natural theoretical framework for a quantitative description of the properties of atoms and molecules. Classical mechanics should however not be completely discarded. In the last decades, sophisticated concepts have emerged that provide a geometric view of the dynamics while bifurcation theory taught us the central role of singularities. The relevance of the quantum-classical correspondence for a qualitative understanding of quantum systems has been pointed out in Refs. [1, 2], where previously unnoticed important features in the quantum analogue of the classical systems were revealed. This approach proves useful for the global analysis of completely integrable few-body models. The exact Hamiltonians of atoms or molecules do not naturally belong to this category but their important qualitative features are reproduced by integrable approximations.

The integrals of motion of completely integrable systems define a singular fibration of the classical phase space and the equations of motion take their simplest expression in locally defined action-angle coordinates. Duistermaat [3] and Cushman [4, 5] introduced the concept of Hamiltonian monodromy which is an obstruction to the global definition of action-angles variables. Many completely integrable models of atomic and molecular systems with two or three degrees of freedom are known to have monodromy [6, 7]. This property

exists in the coupling of two or three angular momenta [8, 9], in some floppy molecules described by spherical pendulum-like models [5], in the Lagrange top [10], in the bottle champagne potential [11, 12] which is akin to the bending motion of quasi-linear molecules (see also Ref. [13]), in the hydrogen atom in electromagnetic fields [14–17], in the problem of two fixed centers [18] describing  $\text{H}_2^+$  and  $\text{HHe}^{2+}$  molecular ions, and in the three-dimensional elastic pendulum [19–21] which is a model for the 1 : 1 : 2 resonance of the carbon dioxide.

The singularities worth the consideration in physics are the structurally stable ones [22, 23], that is, singularities that are still present after a small perturbation of the system. Hamiltonian monodromy gives an example: it originates from the existence of a pinched torus in the phase space and this phenomenon persists under a small perturbation. It may happen that a singularity of a system is unstable under a perturbation but is structurally stable in a family of systems. Catastrophe theory helps in classifying the possible changes that may occur in such a family where one or more control parameters comes into play. The main ideas of this theory have been used by Gilmore, Kais and Levine [24] in the study of a one-dimensional system with the cusp catastrophe as the potential energy term of the Hamiltonian. The signatures of the fold and cusp catastrophes were looked for from the classical and quantum mechanical points of view.

The qualitative analysis of completely integrable systems is concerned with global properties such as the filling of the phase space by regular and singular fibers or the typical singularities that are susceptible to appear [25]. The relationship between

---

\*Electronic address: [guillaume.dhont@univ-littoral.fr](mailto:guillaume.dhont@univ-littoral.fr)

the phase space and the set of constants of motion is established through the energy-momentum map [4]. In particular, the Mineur-Liouville-Arnold theorem [26–28] states that the preimage of a regular value in the image of the energy-momentum map consists in at least one torus. The quantum-classical correspondence establishes a relationship between the classical actions variables and the quantum numbers via the Einstein-Brillouin-Kramers quantization of the tori. The set of eigenvalues of the commuting observables (joint spectrum) of the quantum analog of a completely integrable Hamiltonian defines a lattice [29] in the image of the energy-momentum map. Typical images of the energy-momentum map of two degrees of freedom systems with axial symmetry have already been exposed in the literature and we review the simplest typical cases before presenting our new result.

Figure 1(a) illustrates the simplest conceivable open subset in the image of the energy-momentum map: the grey domain contains only regular values that lift to one regular  $\mathbb{T}^2$  torus. The quantum lattice obtained from the quantum analog of the system is superposed on the same figure. This lattice is locally isomorphic to the  $\mathbb{Z} \times \mathbb{Z}$  set and is therefore completely regular. This regularity is confirmed by drawing a series of elementary cells [8] along any closed loop. The example drawn in Fig. 1(a) demonstrates that the initial and final cell are identical.

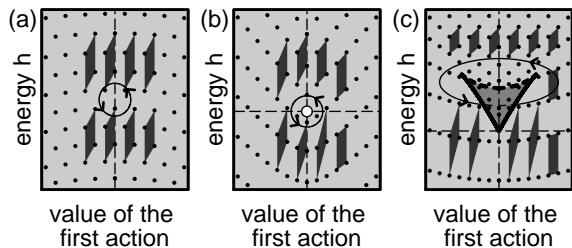


FIG. 1: Typical open subsets of the image of the energy-momentum map for a two degrees of freedom completely integrable system when the first action is a global action. The lattice of dots represents the joint spectrum of commuting observables and the filled quadrilaterals describe the evolution of an elementary cell along one closed loop. (a) Open subset with only regular values. (b) Open subset with regular values and one singular value indicated by the circle. (c) Open subset with two sheets of regular values glued along a singular dashed curve.

A non trivial case is the integer monodromy which is characterized by the existence in the image of the energy-momentum map of an open subset where one critical value for a two degrees of freedom system [see the circle in the center of Fig. 1(b)] or one critical thread for a three de-

grees of freedom system [21] is present. The consequence of monodromy is that any torus bundle over a closed loop of regular values that encircles the singularity is non-trivial. The deformation of elementary cells drawn along this loop shows that the initial and final cells are different: quantum monodromy is interpreted as a defect in the lattice of the joint spectrum [30].

The two previous cases illustrated by Figs 1(a,b) are in some sense elementary, for the preimage through the energy-momentum map of a regular value consists of a unique regular torus. The situation depicted in the integer monodromy case can be deformed to generate a more complex case. The preimage of points in the light grey region of Fig. 1(c) consists of one torus whereas the preimage of points in the dark grey region is composed of two tori. We can draw a parallel between this property and the Riemann surface of multivalued functions in the complex plane: the  $(m, h)$  plane can be organized in *sheets*, such that: (1) the preimage of a regular point of a sheet consists of one and only one regular torus and (2) the torus related to one point of one sheet can be continuously deformed to any other tori associated with points on the same sheet. A first sheet is defined on the whole  $(m, h)$  region visible on Fig. 1(c). The critical value of Fig. 1(b) becomes a finite curve [dashed curve of Fig. 1(c)] and a second sheet of classical values is glued along this curve. The evolution of elementary cells along a closed loop around the dashed curve proves the existence of the so-called nonlocal monodromy. The quantum correspondence of these two sheets of classical values is the superposition of two quantum lattices. Nonlocal monodromy has been proved to exist in the quadratic pendulum [31] and its physical realization, the LiNC/NCLi molecule [32]. The HCN/CNH molecule [33], albeit similar to the LiNC/NCLi case has no monodromy due to the impossibility of defining a loop around the non-local singularity that would go over regular values only, which is a requirement for studying monodromy.

This paper presents a system where two sheets of classical values exist and are glued along a singular curve. However, on the contrary to systems with nonlocal monodromy, *there is no monodromy around the singular curve*. Section II introduces a one-parameter family of completely integrable systems that describes the dynamics of a point mass in a plane. The complete symmetry group of the Hamiltonian is determined and the axial symmetry is used to reduce the dimensionality of the problem. Section III discusses the two canonical forms originating from the fold catastrophe which generically exists in this family. Section IV illustrates these two possible cases with a potential written as an octic polynomial and discusses the quantum-classical correspondence.

## II. A CLASS OF AXIALLY INVARIANT HAMILTONIANS

### A. Mechanical system

A mechanical model of a two degrees of freedom autonomous system may be thought of as a particle of mass  $M$  moving on a plane  $\mathcal{P}$  under the action of conservative forces. The two-dimensional real space  $\mathbb{R}^2$  stands for the configuration space and the Hamiltonian  $\mathcal{H}$  is a scalar function defined on the cotangent bundle  $\mathbb{R}^4$ . The Hamiltonian (1) is assumed to be the sum of a kinetic energy term and an axially symmetric potential:

$$\mathcal{H} : \mathbb{R}^4 \rightarrow \mathbb{R} \quad (1)$$

$$(\tilde{q}_x, \tilde{q}_y, \tilde{p}_x, \tilde{p}_y) \mapsto \frac{\tilde{p}_x^2 + \tilde{p}_y^2}{2M} + \sum_{i=0}^{i_{\max}} b_{2i} (\tilde{q}_x^2 + \tilde{q}_y^2)^i$$

$$(b_{2i_{\max}} > 0).$$

The  $(\tilde{p}_x, \tilde{p}_y)$  pair of variables are the conjugate momenta of the  $(\tilde{q}_x, \tilde{q}_y)$  Cartesian coordinates. The  $b_0$  constant is the first term in the expansion of the potential and plays a trivial role in the Hamiltonian by merely translating the origin of the energy scale and accordingly is set to zero. A scaling transformation  $\tilde{q}_i = \alpha q_i$ ,  $\tilde{p}_i = p_i/\alpha$ ,  $i \in \{1, 2\}$  modify Hamiltonian (1) into the simpler form (2).

$$\mathcal{H} : \mathbb{R}^4 \rightarrow \mathbb{R} \quad (2)$$

$$(q_x, q_y, p_x, p_y) \mapsto \frac{p_x^2 + p_y^2}{2} + \sum_{i=1}^{i_{\max}} c_{2i} (q_x^2 + q_y^2)^i$$

$$(c_{2i_{\max}} = 1).$$

### B. Symmetries of the Hamiltonian

Symmetries simplify the problem at hand and often have fingerprints in the dynamics of the system. The complete symmetry group of Hamiltonian (2) contains both continuous symmetries (rotational symmetry) and discrete symmetries (reflections through a plane containing the  $z$ -axis and the time-reversal operation).

#### 1. Rotational symmetry

The group of rotations  $C_t$  of angle  $t$ ,  $0 \leq t < 2\pi$ , around the third axis  $z$  perpendicular to the plane  $\mathcal{P}$  is isomorph to the  $SO(2)$  group. It induces a transformation (3) between the  $q_x$  and  $q_y$  coordi-

nates and between the  $p_x$  and  $p_y$  momenta:

$$C_t : [0; 2\pi[ \times \mathbb{R}^4 \rightarrow \mathbb{R}^4$$

$$t \times \begin{pmatrix} q_x(0) \\ q_y(0) \\ p_x(0) \\ p_y(0) \end{pmatrix} \mapsto M(t) \begin{pmatrix} q_x(0) \\ q_y(0) \\ p_x(0) \\ p_y(0) \end{pmatrix}, \quad (3a)$$

$$M(t) = \begin{pmatrix} \cos t & -\sin t & 0 & 0 \\ \sin t & \cos t & 0 & 0 \\ 0 & 0 & \cos t & -\sin t \\ 0 & 0 & \sin t & \cos t \end{pmatrix}, \quad (3b)$$

where  $M(t)$  is a block-diagonal rotation matrix. This transformation induces  $2\pi$ -periodic orbits in the phase space and defines a  $\mathbb{S}^1$  group action. The one-parameter continuous symmetry implies by virtue of Noether's theorem that the  $z$ -component of the angular momentum [see Eq. (4)] (simply called angular momentum in the rest of the paper) is a constant of motion.

$$\mathcal{M} : \mathbb{R}^4 \rightarrow \mathbb{R}, (q_x, q_y, p_x, p_y) \mapsto q_x p_y - q_y p_x. \quad (4)$$

#### 2. Plane reflection

The operations  $\sigma_t$  consist of the reflection of the coordinates and momenta through the line  $(Ox)$  rotated by an angle  $t$  around the  $z$ -axis. Equation (5) describes the block-diagonal matrix representation of the transformation.

$$\sigma_t : [0; \pi[ \times \mathbb{R}^4 \rightarrow \mathbb{R}^4$$

$$t \times \begin{pmatrix} q_x(0) \\ q_y(0) \\ p_x(0) \\ p_y(0) \end{pmatrix} \mapsto N(t) \begin{pmatrix} q_x(0) \\ q_y(0) \\ p_x(0) \\ p_y(0) \end{pmatrix}, \quad (5a)$$

$$N(t) = \begin{pmatrix} \cos 2t & \sin 2t & 0 & 0 \\ \sin 2t & -\cos 2t & 0 & 0 \\ 0 & 0 & \cos 2t & \sin 2t \\ 0 & 0 & \sin 2t & -\cos 2t \end{pmatrix}. \quad (5b)$$

#### 3. Time reversal

Hamiltonian (2) is invariant under the time reversal operation  $\mathcal{T}$  which acts as the identity operation on the pair of  $(q_x, q_y)$  coordinates but reverses the sign of the pair  $(p_x, p_y)$  of conjugate momenta:

$$\mathcal{T} : \mathbb{R}^4 \rightarrow \mathbb{R}^4, (q_x, q_y, p_x, p_y) \mapsto (q_x, q_y, -p_x, -p_y).$$

#### 4. Complete symmetry group of the Hamiltonian

The group generated by all products of the  $C_t$  and  $\sigma_t$  operations is isomorphic to the  $C_{\infty v}$  group in the Schönflies notation. The total symmetry group of the Hamiltonian  $\mathcal{H}$  is the direct product  $C_{\infty v} \times \{E, \mathcal{T}\}$ .

### C. Symmetry reduction

The symmetry of the system is now used to transform the initial four-dimensional problem into a two-dimensional problem only. The  $\mathbb{S}^1$  action defines an equivalence relation in phase space. All the points of one orbit are identified to one point of the space of orbits or orbifold [34]. The conservation of the angular momentum restricts the dynamics of the particle and a given value of the constant of motion defines a slice of the orbifold. As a consequence, the final space has two dimensions less than the original phase space.

Equation (3) reveals that the action of the  $SO(2)$  group on the phase space leaves invariant the point at the origin  $(0, 0, 0, 0)$  and the action is therefore not free. The adapted procedure is the singular reduction [4] and is presented in subsection IIC 1. A simpler but less rigorous procedure based on polar coordinates is exposed in subsection IIC 2.

#### 1. Singular reduction

The Hamiltonian (2) is the sum of a kinetic energy quadratic term and of a potential depending only on  $q_x^2 + q_y^2$ . The singular reduction procedure is based on the construction of a ring of  $SO(2)$ -invariant polynomials [35] which are functions of coordinates and conjugate momenta. These invariant polynomials are easily built up in complex coordinates  $z_1 = q_x + iq_y$ ,  $z_2 = p_x + ip_y$  for the effect of the  $SO(2)$  action is equivalent to a multiplication by a phase factor  $e^{\pm it}$ :

$$\begin{cases} z_j \rightarrow e^{it} z_j \\ \bar{z}_j \rightarrow e^{-it} \bar{z}_j \end{cases} \quad j \in \{1, 2\}.$$

The four  $SO(2)$  invariant quadratic polynomials  $R$ ,  $T$ ,  $K$ , and  $L$  are displayed in Table I. We introduce two other polynomials  $X$  and  $Y$  which are linear combinations of the  $T$  and  $R$  polynomials. The syzygy  $X^2 + K^2 + L^2 = Y^2$  shows that the four polynomials  $(X, Y, K, L)$  are algebraically dependent. We consider  $X$ ,  $Y$ , and  $L$  as the principal invariant polynomials and  $K$  as the auxiliary polynomial. Such a choice and the syzygy relation means that any  $SO(2)$ -invariant function can be uniquely decomposed as a linear combination of the polynomials contained in the set  $\{X^p Y^q L^r K^s | (p, q, r) \in \mathbb{N}^3, s \in \{0, 1\}\}$ .

The definition of  $L$  as given by Table I is just half the angular momentum of Eq. (4). The polynomial  $L$  is a constant of the motion for Hamiltonian (2) and is equal to  $m/2$  where  $m$  is the value of the angular momentum. The syzygy relation and the property that  $Y$  is always positive by construction implies that  $Y$  considered as a function of  $X$ ,  $K$  and  $m$  defines a set  $\{S_m\}_{m \in \mathbb{R}}$  of two-dimensional

TABLE I:  $SO(2)$ -invariant polynomials.

	Complex coordinates	Cartesian coordinates
$R$	$\frac{1}{4} z_1 \bar{z}_1$	$\frac{1}{4} (q_x^2 + q_y^2)$
$T$	$\frac{1}{4} z_2 \bar{z}_2$	$\frac{1}{4} (p_x^2 + p_y^2)$
$X$	$\frac{1}{4} (z_2 \bar{z}_2 - z_1 \bar{z}_1)$	$\frac{1}{4} (p_x^2 + p_y^2 - q_x^2 - q_y^2)$
$Y$	$\frac{1}{4} (z_2 \bar{z}_2 + z_1 \bar{z}_1)$	$\frac{1}{4} (p_x^2 + p_y^2 + q_x^2 + q_y^2)$
$K$	$\frac{1}{4} (z_1 \bar{z}_2 + \bar{z}_1 z_2)$	$\frac{1}{2} (q_x p_x + q_y p_y)$
$L$	$\frac{i}{4} (z_1 \bar{z}_2 - \bar{z}_1 z_2)$	$\frac{1}{2} (q_x p_y - q_y p_x)$

reduced phase spaces parameterized by the value of the angular momentum. Figure 2(a) shows that the reduced phase space for  $m = 0$  has a conical-shape singularity at the origin. All the other reduced phase spaces are smooth, as exemplified by Fig. 2(b) for  $m = 2$ . The point at the tip of the  $m = 0$  surface lifts to a single point and all the other points of the  $m = 0$  surface or  $m > 0$  surfaces lift to a circle.

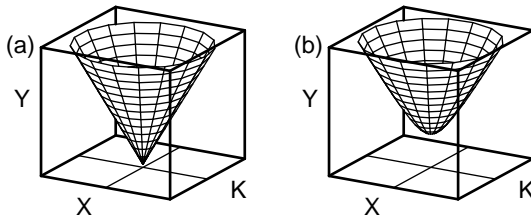


FIG. 2: Reduced phase spaces of a two degrees of freedom  $SO(2)$  invariant Hamiltonian in the space of invariant polynomials  $(X, K, Y)$ . (a) Singular reduced phase space for  $m = 0$ . (b) Smooth reduced phase space for  $m = 2$ .

The behavior of the invariant polynomial upon the time-reversal operation depends on the evenness or oddness of the total degree of the momenta variables. The  $R$ ,  $T$ ,  $X$ , and  $Y$  are invariant whereas the  $K$  and  $L$  polynomials change sign.

#### 2. Polar coordinates

The potential of Hamiltonian (2) is axially symmetric and polar coordinates  $(\rho, q_\varphi)$  and their conjugate momenta  $(p_\rho, p_\varphi)$  decouple the two degrees of freedom. The momentum  $p_\varphi$  is the angular momentum and is a constant of motion which can be replaced by its value  $m$ . In polar coordinates, the Hamiltonian is read as a one-dimensional Hamiltonian:

$$\mathcal{H}_{\text{pol}, m} : \mathbb{R}^+ \times \mathbb{R} \rightarrow \mathbb{R} \quad (\rho, p_\rho) \mapsto \frac{p_\rho^2}{2} + V_{\text{eff}}(\rho; m^2), \quad (6)$$

with an effective potential  $V_{\text{eff}}$

$$V_{\text{eff}}(\rho; m) = \frac{m^2}{2\rho^2} + V_0(\rho), \quad (7a)$$

$$V_0(\rho) = \sum_{i=1}^{i_{\text{max}}} c_{2i} \rho^{2i}. \quad (7b)$$

#### D. Energy-momentum map

##### 1. Definition

The time-independent Hamiltonian (2) is completely integrable and has two integrals of motion (energy and angular momentum). The relation between the initial phase space and the set of constants of motion is described through the energy-momentum map:

$$\begin{aligned} \mathcal{EM}: \mathbb{R}^4 &\rightarrow \mathbb{R}^2 \\ (q_x, q_y, p_x, p_y) &\mapsto \begin{pmatrix} \mathcal{M}(q_x, q_y, p_x, p_y) \\ \mathcal{H}(q_x, q_y, p_x, p_y) \end{pmatrix}. \end{aligned} \quad (8)$$

The relative equilibria (stationary points of the reduced Hamiltonian) are orbits of the action of the  $SO(2)$  symmetry. They are critical values of the energy-momentum map and define parameterized curves in the image of the energy-momentum map [11]. The angular momentum of such relative equilibria is determined by looking for stationary points in the one-dimensional radial effective potential while the term  $h(\rho) = V_{\text{eff}}(\rho; m(\rho))$  gives their energy:

$$\begin{pmatrix} m(\rho) \\ h(\rho) \end{pmatrix} = \begin{pmatrix} \pm \sqrt{\rho^3 \left( \frac{dV_0}{d\rho}(\rho) \right)} \\ V_0(\rho) + \frac{\rho}{2} \frac{dV_0}{d\rho}(\rho) \end{pmatrix},$$

for ranges of  $\rho$  such that  $\frac{dV_0}{d\rho}(\rho) > 0$ .

##### 2. Symmetry

The value of the angular momentum changes sign under the time-reversal operation while the value of the energy is left unchanged. These properties implies that every point  $(m, h)$  in the image of the energy-momentum map has a counterpart  $(-m, h)$  with the angular momentum reversed. We conclude that the image of the energy-momentum map is symmetric with respect to the change of sign of the angular momentum.

### III. FOLD CATASTROPHE IN A FAMILY OF POTENTIALS

#### A. Local description of a potential

##### 1. Noncritical points and Morse critical points

The topology of the potential energy function may have a direct influence on the properties of an Hamiltonian system [36]. A qualitative approach of the local dynamics in the neighborhood of a point of the configuration space is based on the inspection of the first few terms of the Taylor expansion of the potential. Noncritical points and critical points are two qualitatively different types of points that typically exist for a given potential. The gradient of the potential does not vanish at a noncritical point and implies the existence of a force which acts on the particle(s) of the system. An equilibrium is located at a Morse critical point where the gradient and the force vanish but the next term in the Taylor expansion, that is, the quadratic form, is nondegenerate. A Morse critical point persists under a small perturbation even if its position and the value of the function at such a point changes slightly.

##### 2. Degenerate critical points

The quadratic form at a degenerate critical point is degenerate. The degeneracy is partially or completely lifted under a small perturbation and these points are not structurally stable. However, degenerate critical points may generically appear in a family of function when at least one control parameter enter the representation of the function. The fold catastrophe is the simplest case of Thom's elementary catastrophes [22, 23, 37] and the unfolding of its germ requires only one control parameter. The polynomial  $x^3 + \lambda x$  describes the local process of the creation or coalescence of a minimum and a maximum. Fig. 3 illustrates the evolution of the function  $f$  with the parameter  $\lambda$ . The function  $f$  has two extrema when  $\lambda$  is negative and is monotonically increasing for positive  $\lambda$ . The function for  $\lambda = 0$  with a degenerate critical point at the origin marks the transition between these two qualitatively different behaviors.

##### 3. A family of local potentials

We consider the local consequences of a fold catastrophe in a potential  $V_0$  with one control parameter. The local one-dimensional effective potential  $V_{\text{eff}}^{\text{loc},-}$  or  $V_{\text{eff}}^{\text{loc},+}$  is written in the neighborhood of  $\rho_0$  as the sum of a cubic polynomial and a

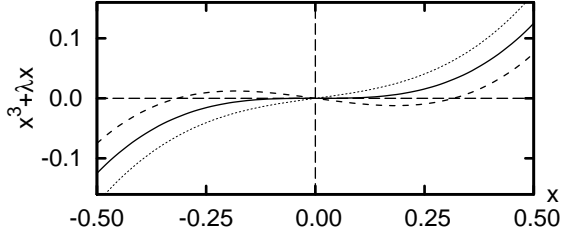


FIG. 3: Fold catastrophe: the germ ( $\lambda = 0$ , solid curve) and its unfolding for  $\lambda = -0.1$  (dashed line) and  $\lambda = 0.1$  (dotted line).

repulsive term:

$$V_{\text{eff}}^{\text{loc},-}(\rho; m; \lambda) = -(\rho - \rho_0)^3 + \lambda(\rho - \rho_0) + \frac{m^2}{2\rho^2}, \quad (9a)$$

$$V_{\text{eff}}^{\text{loc},+}(\rho; m; \lambda) = +(\rho - \rho_0)^3 + \lambda(\rho - \rho_0) + \frac{m^2}{2\rho^2}. \quad (9b)$$

The two parameters  $m$  and  $\lambda$  have distinct physical origins. The reduction with the  $\mathbb{S}^1$  action of the initial axially symmetric Hamiltonian induces a new Hamiltonian where the angular momentum  $m$  appears as a constant of motion through Noether's theorem. As a consequence,  $m$  describes the *internal* dynamics of the system. On the contrary, the parameter  $\lambda$  is an *external* parameter which reflects tunable external forces imposed on the system.

The first two terms of Eq. (9a) and (9b) are similar to the canonical form of the fold catastrophe except for the sign in front of the cubic term. The two possible cases are distinct due to presence of the repulsive term that appears after reduction of the rotational symmetry. This term forbids the symmetry operation  $\rho - \rho_0 \mapsto -(\rho - \rho_0)$  that is performed in canonical catastrophe theory [37]. Subsection III B discusses the consequences of the first case given by Eq. (9a) whereas subsection III C treats the second case described by Eq. (9b).

## B. Case I: appearance of a second sheet

### 1. Critical points in the effective potentials

A stationary point of the effective potential is a relative equilibrium of the original system. The local effective potential of Eq. (9a) is plotted for five values of  $m^2$  on Fig. 4 for three values of  $\lambda$  around and including zero. Fig. 4(a) shows that the effective potentials are decreasing monotonic functions for  $\lambda < 0$  and for any  $m^2$ . They have no stationary points. When the control parameter

vanishes, one degenerate critical point appears at  $\rho = \rho_0$  for the  $m = 0$  thick curve on Fig. 4(b). The effective potentials for all other  $m$  values are decreasing monotonic functions. The situation where  $\lambda > 0$  is the richest, see Fig. 4(c). The effective potential  $V_{\text{eff}}^{\text{loc},-}(\rho; m_{\text{deg},\text{I}}(\lambda); \lambda)$  has a degenerate critical point at  $\rho = \rho_{\text{deg},\text{I}}(\lambda)$ . This curve separates the potentials with  $m < m_{\text{deg},\text{I}}(\lambda)$  that have one minimum and one maximum from the potentials with  $m > m_{\text{deg},\text{I}}(\lambda)$  that are decreasing monotonic functions and have no stationary points. Using the property that both first and second derivatives vanish at the critical point, we find the position, the angular momentum, and the energy of this point as a function of the control parameter  $\lambda$ :

$$\rho_{\text{deg},\text{I}}(\lambda) = \left( 4 + \sqrt{1 + 5 \frac{\lambda}{\rho_0^2}} \right) \frac{\rho_0}{5}, \quad (10a)$$

$$m_{\text{deg},\text{I}}^2(\lambda) = -\frac{2}{3125} \left( 1 - \sqrt{1 + 5 \frac{\lambda}{\rho_0^2}} \right) \times \left( 4 + \sqrt{1 + 5 \frac{\lambda}{\rho_0^2}} \right)^4 \rho_0^5, \quad (10b)$$

$$h_{\text{deg},\text{I}}(\lambda) = V_{\text{eff}}^{\text{loc},-}(\rho_{\text{deg},\text{I}}(\lambda); m_{\text{deg},\text{I}}(\lambda); \lambda). \quad (10c)$$

We note from Eq. (10a) that the position of the degenerate critical point (which exists only for  $\lambda \geq 0$ ) is an increasing function of  $\lambda$ . We conclude that in general, the effective potential has no stationary point, except for the important case where  $\lambda$  is positive and the angular momentum is less than the critical value  $m_{\text{deg},\text{I}}(\lambda)$ .

### 2. Reduced phase space and tori

The axially symmetric Hamiltonian with potential (9a) is a function of the invariant polynomials  $T$  and  $R$  or, equivalently, a function of the invariant polynomials  $X$  and  $Y$ . The levels sets  $H(X, Y) = h$  of the Hamiltonian define a family of two-dimensional surfaces  $S_h$  parameterized by the energy  $h$  in the three-dimensional space  $(X, K, Y)$ . The invariant tori of the initial phase space  $\mathbb{R}^4$  are reconstructed for a given angular momentum  $m$  and energy  $h$  from the intersection  $I_{m,h}$  between the surface  $S_m$  of the reduced phase space and the surface  $S_h$  of the energy level set [4]. The parameterization of  $S_h$  does not depend on the polynomial  $K$  and it is convenient to project both  $S_m$  and  $S_h$  surfaces on the  $(X, Y, K = 0)$  plane. The grey domains  $\mathcal{D}_m$  of Fig. 5 are projections of the  $S_m$  surface on the  $K = 0$  plane while the projection of the  $S_h$  surface is drawn as a dotted curve  $\mathcal{C}_h$ . The projection of the intersection  $I_{m,h}$  is the part of the curve  $\mathcal{C}_h$  contained in the domain  $\mathcal{D}_m$ . A

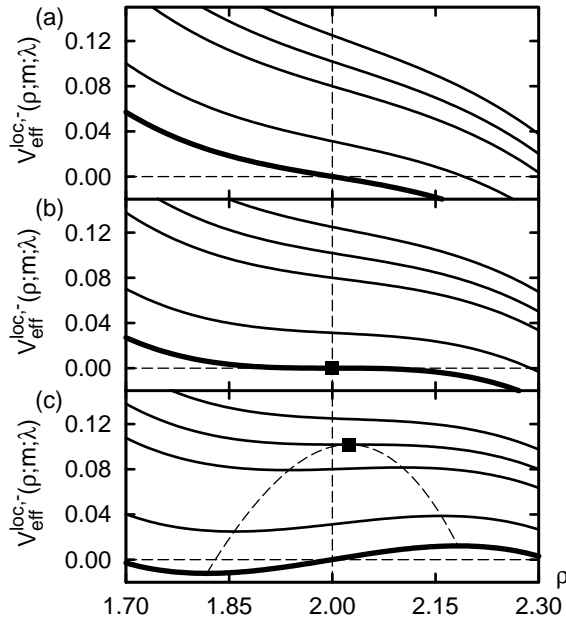


FIG. 4: Local effective potential  $V_{\text{eff}}^{\text{loc},-}(\rho; m; \lambda)$  for  $\rho_0 = 2$  and a fixed set of five values of angular momentum  $m$ . The effective potential with  $m = 0$  is represented by a thick curve. Angular momentum increases (values:  $m_1 = 0.5, m_2 = 0.8, m_{\text{deg},1}(0.1) \simeq 0.903, m_3 = 1.0$ ) when jumping from one potential curve to the upper one. Filled squares indicate degenerate critical points. (a) Control parameter  $\lambda = -0.1$ . (b) Control parameter  $\lambda = 0$ . (c) Control parameter  $\lambda = 0.1$ . Positions of the minima and maxima of the effective potentials are indicated by the dashed curves.

point of  $\mathcal{C}_h$  inside the domain  $\mathcal{D}_m$  is the projection of two points of  $I_{m,h}$  while a point of  $\mathcal{C}_h$  on the border of the domain  $\mathcal{D}_m$  corresponds to only one point of  $I_{m,h}$ .

The local character of the fiber, *i.e.* regular or singular, is determined by how the energy level set crosses the reduced phase space. The crossing pictured on Fig. 5(a,b) is the typical situation associated with a locally regular torus and happens when the gradients of the two surfaces differ at the intersection point. First-order and higher-order points occur when the two surfaces  $S_h$  and  $S_m$  are locally tangent. The gradients at the intersection point are identical and the difference between the two surfaces requires a higher order Taylor expansion. In such situations, the difference between the two surfaces near this point may be quadratic [Fig. 5(c-f)], cubic [Fig. 5(g,h)] or even higher. The intersection on Fig. 5(c,d) is locally reduced to the point marked by a diamond and corresponds to a  $\mathbb{S}^1$  circle in the initial phase space. Fig. 5(e,f) illustrates the situation when the projected intersection  $I_{m,h}$  is identical to the full energy level set near the contact point marked by the triangle. The fiber is in this case locally diffeomorphic to a bitorus. The

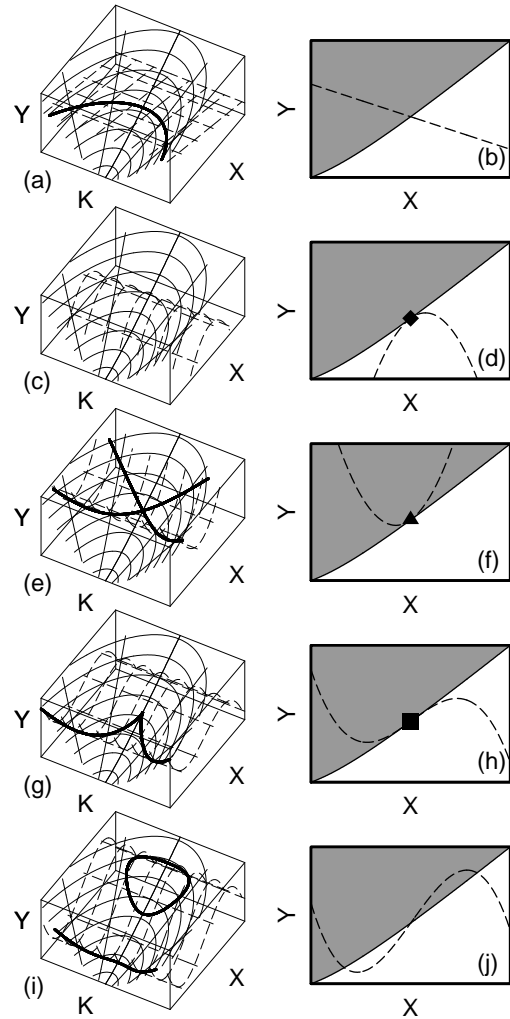


FIG. 5: Five different cases of intersections between the reduced phase spaces and the energy level sets. Left column: three dimensional view in the  $(X, K, Y)$  space of invariant polynomials. The surfaces drawn in continuous curves are the reduced phase spaces and the level sets of the energy are drawn with dashed lines. The intersections of these two surfaces are drawn as thick curves whose individual points lift up to  $\mathbb{S}^1$  circles. Right column: projection of the reduced phase space (grey domain) and the projection of the energy level sets (dashed curves) in the  $(X, Y)$  space of invariant polynomials. (a,b) Regular intersection. (c,d) First-order contact point,  $\mathbb{S}^1$  intersection. (e,f) First-order contact point, locally bitorus-like intersection. (g,h) Second-order contact point, locally cuspidal-like intersection. (i,j) Three regular intersections.

square on Fig. 5(h) is a second-order contact point. The corresponding fiber is not locally regular as in Fig. 5(a,b) but has a singular line and is called a cuspidal torus [38, 39]. Finally, a case where more than one regular intersection may occur, as pictured in Fig. 5(i,j). The rightmost part of the energy level set in the grey domain of Fig. 5(j) lifts up to a complete regular torus whereas the left-

most part lifts up to a locally regular torus.

Figure 6 shows the projection of reduced phase space surfaces and energy level sets on the  $K = 0$  plane obtained from potential (9a) for several values of the control parameter  $\lambda$  and angular momentum  $m$ . The vertical axis shows the sum of the two invariant polynomials  $X$  and  $Y$ : this choice, rather than the natural choice of  $Y$  as in Fig. 5, is only made for a better legibility of the figure. Most of the fibers are regular  $\mathbb{T}^2$  tori and the interesting fibers are naturally the singular ones. All the fibers are regular  $\mathbb{T}^2$  tori when  $\lambda < 0$ . This situation persists for  $\lambda = 0$ , except for one fiber which is locally similar to a cuspidal torus, see Fig. 6(b). The last two figures show for  $\lambda > 0$  three examples of singular fibers similar to those presented on Figs. 5(c-h), that is, a  $\mathbb{S}^1$  degenerate torus and a locally bitorus-like fiber [Fig. 6(c)] and a locally cuspidal-like fiber [Fig. 6(d)].

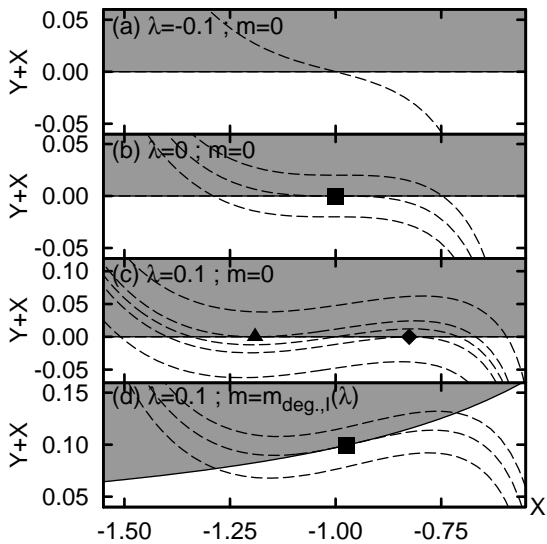


FIG. 6: Projections of the reduced phase spaces (grey domains) and energy level sets (dashed curves) in the  $(X, Y+X)$  space of invariant polynomials for the case I with  $\rho_0 = 2$ . The symbols of Fig. 5 are used to label the singular intersection points.

It should be noted that the time-reversal operation changes the sign of the value of the angular momentum and distinguishes the two cuspidal tori that exist when  $\lambda > 0$  from the cuspidal torus that appears for  $\lambda = 0$ . This operation maps for  $\lambda > 0$  a cuspidal torus to the cuspidal torus with opposite angular momentum whereas time-reversal maps the cuspidal torus for  $\lambda = 0$  to itself. As a consequence, the invariance group of the  $\lambda = 0$  cuspidal torus is bigger than the invariance group of one  $\lambda > 0$  cuspidal torus.

### 3. Image of the energy-momentum map

The understanding of the foliation of the phase space by regular and singular fibers is improved with the concept of the energy-momentum map. Images of the energy-momentum map  $\mathcal{EM}$  are presented on Fig. 7 for three values of  $\lambda$ . The left-right symmetry is a direct consequence of the symmetry mentioned in Sec. IID 2. The preimage of some selected points is pictured on the left and right sides of the figure. The Hamiltonian of Eq. (6) gives a relationship between  $\rho$  and  $p_\rho$  that is useful for visualizing invariant tori:

$$h = \frac{p_\rho^2}{2} + V_{\text{eff}}^{\text{loc},-}(\rho; m; \lambda).$$

The radial conjugate momenta is a function of  $h$ ,  $m$ , and  $\rho$ . Due to the rotational symmetry, we can suppose  $y = 0$  and represent  $p_\rho$  as a function of  $x$ .

Figure 7(a) clearly indicates that only one sheet exists for  $\lambda < 0$ . A point  $(m, h)$  inside the sheet corresponds to one locally regular torus  $\mathbb{T}^2$ . The description of the situation for  $\lambda = 0$  is the same, see Fig. 7(b), except for the appearance of a particular point at the origin. The preimage of this point is a locally cuspidal-like torus at  $(m = 0, h = 0)$ . Figure 7(c) shows that the situation for  $\lambda > 0$  is more complex: the light grey domain is a region where each point lifts through the energy-momentum map to one locally regular torus  $\mathbb{T}^2$ , whereas the dark grey domain is a region where each point lifts to two different locally regular tori  $\mathbb{T}^2 \cup \mathbb{T}^2$ . Note that one of these two tori can be continuously deformed to any regular torus associated with the light grey domain. This property strongly advocates the definition of a first sheet such that its domain is the whole  $(m, h)$  region of Fig. 7(c). The remaining tori, the ones that cannot be continuously deformed to a torus in the light grey domain, are associated with a second sheet whose region is restricted to the grey domain. The two sheets are glued together along the dashed curve, which is a set of critical values. The preimage of each of these values is a locally bitorus-like fiber, where two tori are glued along one singular line. The remaining border of the second sheet consists of points that each lifts to a  $\mathbb{S}^1$  circle (a degenerate torus).

The main conclusion in case I is that *a second sheet appears as  $\lambda$  becomes positive*.

### C. Case II: breaking of the second sheet

#### 1. Critical points in effective potentials

The same methodology as above is pursued to discuss the consequences of Eq. (9b) on the folia-

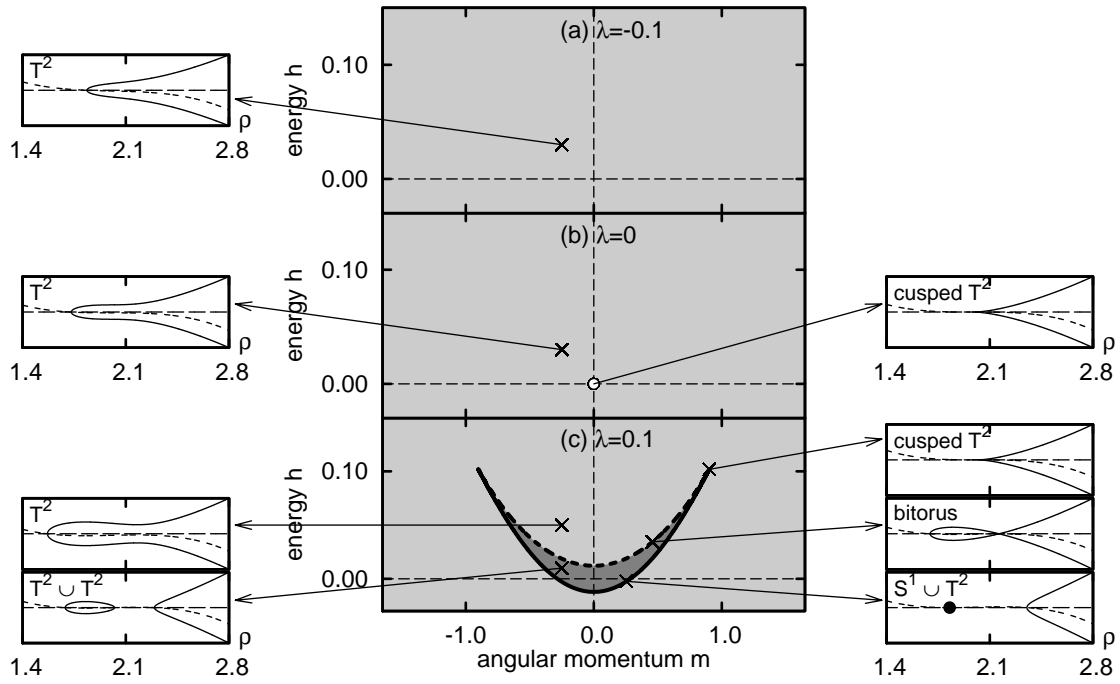


FIG. 7: Images of the energy-momentum map in case I. The preimage of a point in the light grey areas is one torus while the preimage of a point in the dark grey area consists of two tori. Selected points in the image of the energy-momentum map are marked by a cross and the figures attached to them show the effective potential (dashed curve), the energy (horizontal dashed curve), and the conjugate momenta  $p_\rho$  (solid curve). (a) Control parameter  $\lambda = -0.1$ . (b) Control parameter  $\lambda = 0$ . (c) Control parameter  $\lambda = 0.1$ .

tion of the phase space. The local effective potentials pictured on Fig. 8 show that the situation is opposite to Fig. 4: the potentials with one minimum and one maximum are now the rule, except when  $\lambda$  is positive and  $m < m_{\text{deg,II}}(\lambda)$  where the potential is a monotonic increasing function of  $\rho$ . Curves with a degenerate critical point appear only for  $\lambda \geq 0$ . A degenerate critical point appears exactly at  $\rho = \rho_0$  for  $\lambda = 0$  and Eq. (11a) states that this point moves towards smaller values of  $\rho$  when  $\lambda$  increases. Note that this effect is the opposite to case I.

$$\rho_{\text{deg,II}}(\lambda) = \left(4 + \sqrt{1 - 5\frac{\lambda}{\rho_0^2}}\right) \frac{\rho_0}{5}, \quad (11a)$$

$$m_{\text{deg,II}}^2(\lambda) = \frac{2}{3125} \left(1 - \sqrt{1 - 5\frac{\lambda}{\rho_0^2}}\right) \times \left(4 + \sqrt{1 - 5\frac{\lambda}{\rho_0^2}}\right)^4 \rho_0^5, \quad (11b)$$

$$h_{\text{deg,II}}(\lambda) = V_{\text{eff}}^{\text{loc,+}}(\rho_{\text{deg,II}}(\lambda); m_{\text{deg,II}}(\lambda); \lambda). \quad (11c)$$

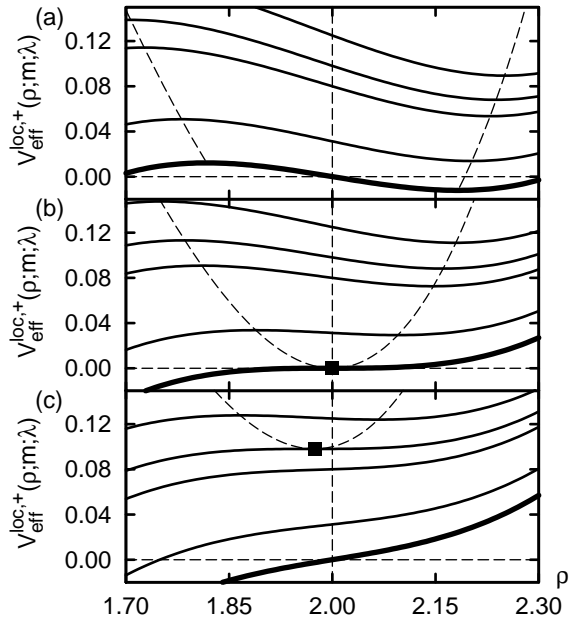


FIG. 8: Local effective potential  $V_{\text{eff}}^{\text{loc,+}}(\rho; m; \lambda)$  for  $\rho_0 = 2$  and a fixed set of five values of angular momentum  $m$ . The effective potential with  $m = 0$  is represented by a thick curve. Angular momentum increases (values:  $m_1 = 0.5, m_2 = 0.8, m_{\text{deg,II}}(0.1) \simeq 0.886, m_3 = 1.0$ ) when jumping from one potential curve to the upper one. Filled squares indicate degenerate critical points. Positions of the minima and maxima of the effective potentials are indicated by the dashed curves. (a) Control parameter  $\lambda = -0.1$ . (b) Control parameter  $\lambda = 0$ . (c) Control parameter  $\lambda = 0.1$ .

## 2. Reduced phase space and tori

Figure 9 is the counterpart for the potential (9b) of Fig. 6. The most striking difference with case I is the existence of  $\mathbb{S}^1$  degenerate tori and locally bitorus-like fibers even for negative values of the control parameter, as shown on Fig. 9(a) and Figs. 9(c-d). However, the appearance of locally cuspidal-like tori only occurs for  $\lambda \geq 0$  [see Fig. 9(b) and Fig. 9(e)] exactly as in case I.

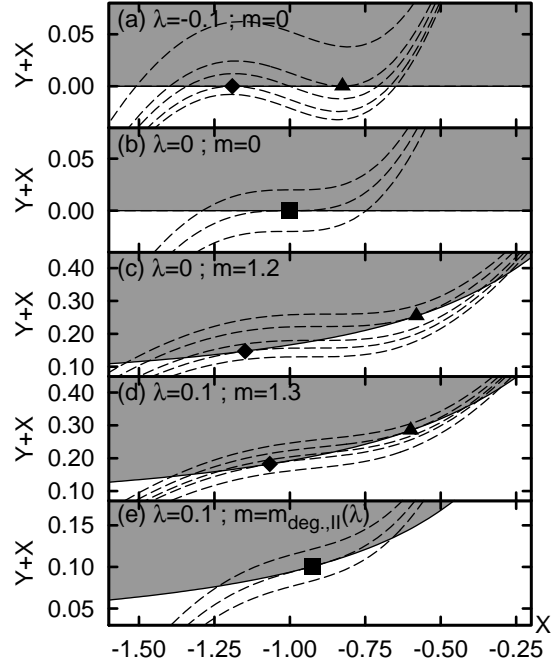


FIG. 9: Projections of the reduced phase spaces (grey domains) and energy level sets (dashed curves) in the  $(X, Y + X)$  space of invariant polynomials for the case II with  $\rho_0 = 2$ . The symbols of Fig. 5 are used to label the singular intersection points.

## 3. Image of the energy-momentum map

The images of the energy-momentum map on Fig. 10 are fundamentally different from those pictured in Fig. 7 for case I. We do not see anymore the creation or annihilation of a second sheet but rather observe the breaking of a sheet into two symmetric sheets. This symmetry comes from the left-right symmetry of the image of the energy-momentum map. A point in the light grey domain is associated with one regular torus  $\mathbb{T}^2$  whereas a point in the dark grey domain is associated with two different regular torus  $\mathbb{T}^2 \cup \mathbb{T}^2$ . The continuity argument among the tori of case I is employed again to define two different sheets: a first sheet that covers the whole Fig. 10(c) and a second one

that covers the dark grey domain. The preimage of a point in the upper boundary (dashed curve) of the second sheet is a locally bitorus-like fiber. The preimage of a point in the lower boundary of the second sheet is a  $\mathbb{S}^1$  circle. Figures 10(b-c) show that these upper and lower boundaries intersect for  $\lambda \geq 0$  and the preimage of the intersection point is a locally cuspidal-like torus.

We conclude that in case II as  $\lambda$  becomes positive, the domain with two sheets breaks into two symmetric domains with two sheets each.

#### D. Structural stability

The effects of a fold catastrophe in a one-dimensional effective potential were discussed in IIIB and IIIC. We now prove that the phenomenon is structurally stable and persists under a small perturbation of the system, which is a requirement for this phenomenon to be of physical importance.

##### 1. Family of effective potentials

We consider a family of one-dimensional effective potentials depending on the variable  $\rho$  and two parameters:  $m^2$  and  $\lambda$ :

$$V_{\text{eff}}(\rho; m; \lambda) = V_0(\rho) + \frac{m^2}{2\rho^2} + \lambda F(\rho), \quad (12)$$

where  $V_0(\rho)$  is the potential of the system and  $F$  is a function.

We suppose that a degenerate critical point occurs at  $(\rho = \rho_0, m = 0, \lambda = 0)$  and we accordingly rewrite the potential as:

$$V_{\text{eff}}(\rho; m; \lambda) = V_0(\rho_0) + (\rho - \rho_0)^3 W(\rho) + \frac{m^2}{2\rho^2} + \lambda F(\rho),$$

with  $W(\rho_0) \neq 0$ . The constant  $V_0(\rho_0)$  is nonessential and may be dropped.

For  $\lambda$  nonzero, we find the position of the degenerate critical point and the angular momentum using a Newton's method:

$$\begin{cases} \rho_{\text{deg}} = \rho_0 - \frac{3 \frac{dF}{d\rho}(\rho_0) + \rho_0 \frac{d^2 F}{d\rho^2}(\rho_0)}{6\rho_0 W(\rho_0)} \lambda + O(\lambda^2), \\ m_{\text{deg}}^2 = \rho_0^3 \frac{dF}{d\rho}(\rho_0) \lambda + O(\lambda^2). \end{cases}$$

For small enough  $\lambda$ , the sign of  $m_{\text{deg}}^2$  is the same as  $\frac{dF}{d\rho}(\rho_0)\lambda$ . We suppose  $\frac{dF}{d\rho}(\rho_0)$  is positive. We can always redefine the external parameter  $\lambda$  and the external function  $F$  if this does not hold. When  $\lambda$  is negative, no cuspidal points can exist whereas two cuspidal points exist for  $m \neq 0$  for positive  $\lambda$ .

##### 2. Perturbation

We consider equivariant perturbations, that is, perturbative functions that have the axial symmetry of the original problem and add a perturbative term to the effective potential. Catastrophe theory establishes that one parameter is necessary and sufficient for the fold catastrophe to occur in a family of one-dimensional potentials. The existence of this degenerate critical point is structurally stable: the fold catastrophe persists under a perturbation of the potential whereas the values of the parameter and the position of the singular point are slightly changed.

The unperturbed effective one-dimensional potential depends on one internal parameter  $m$  and one external parameter  $\lambda$ . A degenerate critical point exists for the unperturbed local potential when both internal and external parameters vanish. Keeping fixed the angular momentum at  $m = 0$ , the perturbation merely shifts the position of the degenerate critical point which appears at  $\lambda = \lambda_{\text{deg}}^*$ . The qualitative description of the unfolding of the fold catastrophe at  $(m = 0, \lambda = 0)$  remains valid at  $(m = 0, \lambda = \lambda_{\text{deg}}^*)$ . The phenomena presented in this paper are henceforth stable under any small equivariant perturbation.

## IV. FOLD CATASTROPHE IN OCTIC POTENTIALS

### A. Family of Hamiltonians

Section III discussed the local changes induced by a fold catastrophe in the fibration of the phase space for a family of axially symmetric Hamiltonians. This section deals with the consequences of a fold catastrophe in a family of systems described by Eq. (6) with an octic potential defined on the real half-line:

$$\begin{aligned} V_{\text{oct}}(\rho; \mu) = & \rho^8 - \frac{4}{3}(\rho_2^2 + 2\rho_1^2)\rho^6 \\ & + 2(2\rho_1^2\rho_2^2 + \rho_1^4 - \mu)\rho^4 \\ & - 4\rho_2^2(\rho_1^4 - \mu)\rho^2. \end{aligned} \quad (13)$$

The potential is parameterized by a control parameter  $\mu$  and two positive constants  $\rho_1$  and  $\rho_2$ . Table II lists the relative equilibria of the system for  $m = 0$  (extrema of the potential  $V_{\text{oct}}$ ) and it can be inferred from the appearance of two new critical points for  $\mu \geq 0$  that a cusp catastrophe occurs in this family of potentials at  $\rho = \rho_1$ . This behavior with increasing control parameter is the same as the one observed on Fig. 4 with the potential  $V_{\text{eff}}^{\text{loc},-}$  and vanishing angular momentum but reverses the sequence of events obtained in Fig. 8

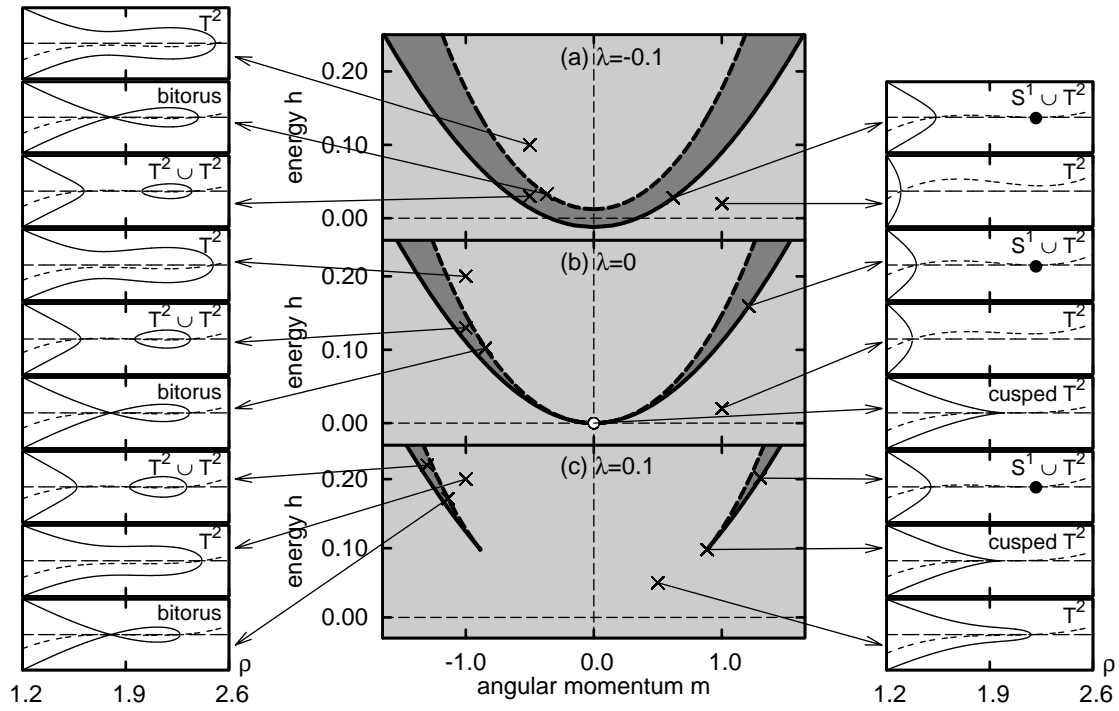


FIG. 10: Images of the energy-momentum map in case II. The preimage of a point in the light grey areas is one torus while the preimage of a point in the dark grey areas consists of two tori. Selected points in the image of the energy-momentum map are marked by a cross and the figures attached to them show the effective potential (dashed curve), the energy (horizontal dashed curve), and the conjugate momenta  $p_\rho$  (solid curve). (a) Control parameter  $\lambda = -0.1$ . (b) Control parameter  $\lambda = 0$ . (c) Control parameter  $\lambda = 0.1$ .

from  $V_{\text{eff}}^{\text{loc},+}$ . We should expect in this second situation the breaking of the second sheet when the control parameter *decreases*.

TABLE II: Positions of the extrema of the octic potential  $V_{\text{oct}}$  defined in Eq. (13).

Sign of $\mu$	Positions of extrema
$\mu < 0$	$0, \rho_2$
$\mu = 0$	$0, \rho_2, \rho_1, \rho_1$
$\mu > 0$	$0, \rho_2, \sqrt{\rho_1^2 - \sqrt{\mu}}, \sqrt{\rho_1^2 + \sqrt{\mu}}$

The potential  $V_{\text{oct}}$  is expanded in Taylor series at  $\rho = \rho_1$  as:

$$V_{\text{oct}}(\rho; \mu) = V_0 + V_1(\rho - \rho_1) + V_2(\rho - \rho_1)^2 + V_3(\rho - \rho_1)^3 + \mathcal{O}((\rho - \rho_1)^4) \quad (14)$$

with

$$V_0 = \frac{1}{3}\rho_1^6(\rho_1^2 - 4\rho_2^2) - 2\mu\rho_1^2(\rho_1^2 - 2\rho_2^2) \quad (15a)$$

$$V_1 = -8\mu\rho_1(\rho_1 - \rho_2)(\rho_1 + \rho_2), \quad (15b)$$

$$V_2 = 4\mu(\rho_2^2 - 3\rho_1^2), \quad (15c)$$

$$V_3 = \frac{32}{3}\rho_1^3(\rho_1 - \rho_2)(\rho_1 + \rho_2) - 8\mu\rho_1. \quad (15d)$$

The terms  $V_1$  and  $V_2$  in front of the linear and quadratic terms of the Taylor expansion are proportional to the control parameter  $\mu$ . These two terms vanish at  $\mu = 0$  and the potential  $V_{\text{oct}}$  has a degenerate critical point at  $\rho = \rho_1$ . Catastrophe theory states the existence of a nonlinear transformation that casts Eq. (14) in the canonical form  $V_0 \pm (\tilde{\rho} - \tilde{\rho}_0)^3 + \lambda(\mu, V_1, V_2, V_3, \dots)(\tilde{\rho} - \tilde{\rho}_0)$  of a fold catastrophe, where  $\lambda$  is a function of the parameter  $\mu$  and of the coefficients  $V_i$ . The potential  $V_{\text{oct}}$  is defined on the real half-line and the two possible signs in front of the cubic term are therefore inequivalent. The sign of  $\rho_1 - \rho_2$  determines the sign of  $V_3$  in front of the cubic term of Eq. (14) for  $\mu$  small enough and discriminates between the two cases of Section III.

### B. Monodromy

A noteworthy feature of the family of potentials  $V_{\text{oct}}$  is its behavior near the origin  $\rho = 0$ . The quadratic term dominates and is negative for  $\mu$  small enough, which makes this potential locally similar to the so-called bottle champagne or Mexican hat potential [11, 12]. The value  $(m = 0, h = 0)$  is a singular value of the energy-momentum map and its preimage is a pinched torus. This singular fiber makes impossible the global definition of action-angle variables and induces a local defect

in the lattice of quantum eigenstates. The rest of the paper focuses on the dynamics for negative energies only. The image of the energy-momentum map for a control parameter  $\mu$  is noted  $\mathcal{D}_\mu$  and the restriction to negative energy values defines the subset  $\mathcal{D}_{\mu, h < 0} = \{(m, h) | (m, h) \in \mathcal{D}_\mu, h < 0\}$ .

### C. Case $\rho_2 > \rho_1$ : appearance of a second sheet

We first deal with the situation where  $\rho_2 > \rho_1$ . Figure 11 shows, for three different values of the control parameter  $\mu$ , the image of the energy-momentum map and the octic potential  $V_{\text{oct}}$ . The small dots represent the lattice of quantum eigenstates obtained by solving the time-independent Schrödinger equation in a two-dimensional harmonic oscillator basis [12, 40]. The Heisenberg uncertainty and the zero-point energy imply that this joint spectrum is completely inside the classical domain of the energy-momentum map. The succession of events occurring in  $\mathcal{D}_{\mu, h < 0}$  with increasing  $\mu$  is the same as the local model of Eq. (9a). All the values in  $\mathcal{D}_{\mu, h < 0}$  are regular when the control parameter is negative and corresponds quantum mechanically to the regularity of the lattice in this region.

The open circle in Fig. 11(b) corresponds to the singular value originating from the fold catastrophe which appears when the control parameter vanishes. The enlargement of an open set containing this singularity is pictured on Fig. 12(a). The displacement of an elementary cell around this singularity indicates that the final cell can be superposed to the initial cell and is related to the absence of monodromy in  $\mathcal{D}_{\mu, h < 0}$ . Fig. 11(c) is marked by the presence of a second sheet in the positive control parameter case. The point-like singularity has become a singular line and once again the displacement on an elementary cell around this line in Fig. 12(b) proves that there is no monodromy in  $\mathcal{D}_{\mu, h < 0}$ . The appearance of a second sheet in  $\mathcal{D}_{\mu, h < 0}$  does not alter the regularity of the quantum lattice.

### D. Case $\rho_2 < \rho_1$ : reversed breaking of the second sheet

We now deal with the situation where  $\rho_2 < \rho_1$ . The joint spectra of the quantum system superposed on the image of the energy-momentum maps are drawn on Fig. 13 for three different values of the parameter  $\mu$ . The three insets represent the one-dimensional potential  $V_{\text{oct}}$  for the corresponding values of the control parameter. The number of extrema increases from one to three via a fold catastrophe at  $\mu = 0$ . The possible monodromy is usually searched for with a closed loop that en-

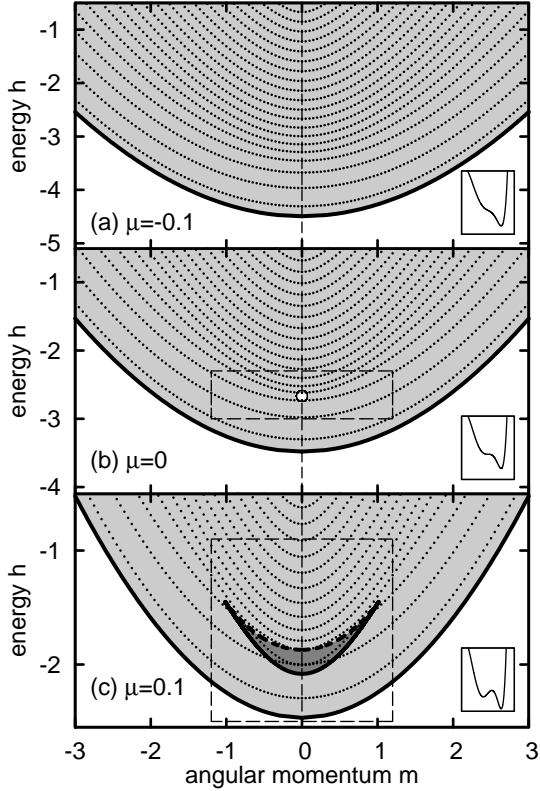


FIG. 11: Images of the energy-momentum map obtained from the octic potential  $V_{\text{oct}}$  [Eq. (13)] for  $\rho_1 = 1.0$  and  $\rho_2 = 1.5$ . The joint spectrum of commuting observables is represented by small dots and is determined with the Planck constant set to  $\hbar = 0.05$ . The insets show the octic potential  $V_{\text{oct}}$ . (a) Control parameter  $\mu = -0.1$ . (b) Control parameter  $\mu = 0$ . The dashed rectangle delimits the area that is enlarged in Fig. 12(a). (c) Control parameter  $\mu = 0.1$ . The dashed rectangle delimits the area that is enlarged in Fig. 12(b).

circles a singularity and which passes through only regular values in  $\mathcal{D}_{\mu, h < 0}$ . Such a loop is impossible to construct for any of the three energy-momentum maps of Fig. 13 and the concept of monodromy is not relevant for the case  $\rho_2 < \rho_1$ .

Fig. 13(a) has nevertheless interesting properties and an enlargement of the energy-momentum map between  $m = 2.1$  and  $m = 2.6$  is presented on Fig. 14(a) where a shift of the energy scale by a linear function of  $m$  has been performed. The points in the light grey region of the image of the energy-momentum map lift up to one torus while the points in the dark grey region lift up to two tori. A similar figure has been discussed by Sadovskii and Zhilinskii in relation with the manifestation of bidromy, see Fig. 18 of Ref. [41]. Figures 14(b-k) show the effective potential, the energy, and the radial momentum  $\pm p_\rho(\rho)$  for ten  $(m, h)$  selected points. The plot of the radial momentum as a function of the radial coordinate gives a good indi-

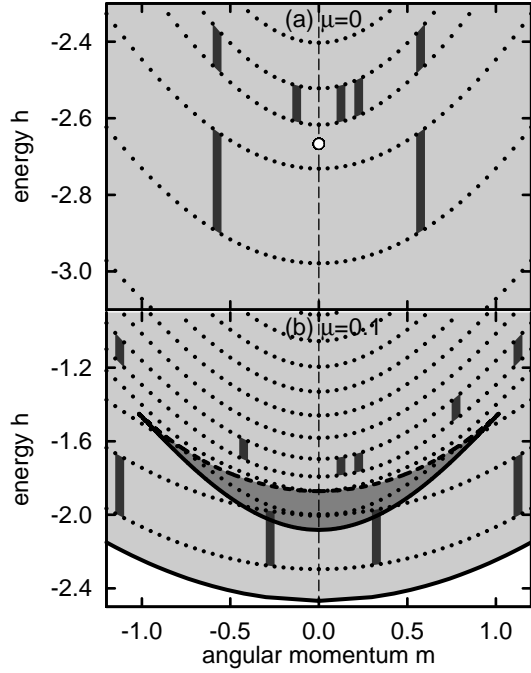


FIG. 12: (a) Enlargement of Fig. 11(b) in the vicinity of the singularity. (b) Enlargement of the two sheets seen on Fig. 11(c).

cation of the shape of the torus. We consider now a continuous transformation of tori while traveling counterclockwise on the loop represented on Fig. 14(a): it begins from the point attached to Fig. 14(b) and terminates at the point attached to Fig. 14(k). These two points are identical in the image of the energy-momentum map but a comparison between Fig. 14(b) and Fig. 14(k) reveals that we can continuously pass from the torus on the right of Fig. 14(b) (the torus where the radial coordinate is higher) to the torus on the left.

We start with the point attached to Fig. 14(b) from the torus located at the right and move continuously on the loop. The torus on the left gets smaller until the point attached with Fig. 14(c) is met where this torus finally degenerates to a  $\mathbb{S}^1$  circle in the phase space. The points attached with Figs. 14(d-i) are in the light grey domain of Fig. 14(a) and only one torus appears on each of Figs. 14(d-i). Figure 14(j) is marked by the appearance of a circle in the phase space which develops afterwards as a second torus. Comparing Fig. 14(b) and Fig. 14(k), we see that one of the two torus has been continuously transformed to the other one. Two regular quantum lattices are superposed in the dark grey region and the continuous loop presented above indicates that it is possible to pass from one lattice into the other one, which means that these two parts belong to the same regular self-overlapping lattice.

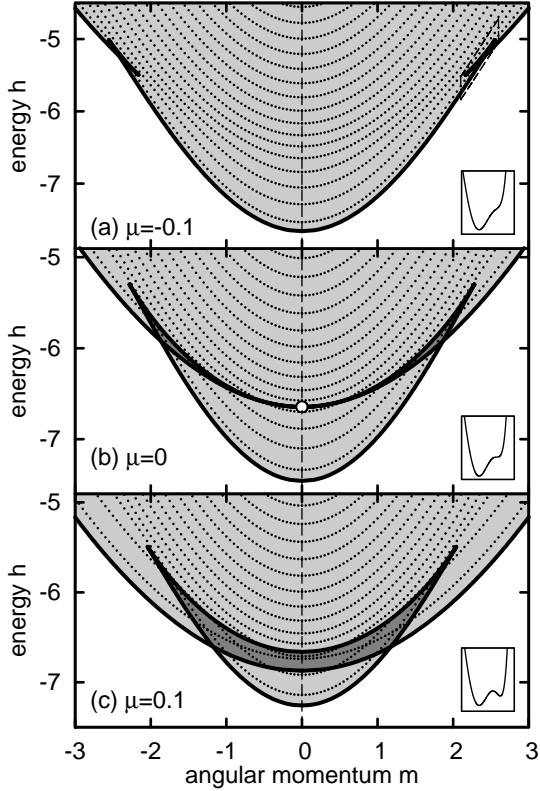


FIG. 13: Images of the energy-momentum map obtained from the octic potential  $V_{\text{oct}}$  [Eq. (13)] for  $\rho_1 = 1.5$  and  $\rho_2 = 1.0$ . The joint spectrum of commuting observables is represented by small dots and is determined with the Planck constant set to  $\hbar = 0.05$ . The insets show the octic potential  $V_{\text{oct}}$ . (a) Control parameter  $\mu = -0.1$ . The dashed curves delimit the area that is enlarged in Fig. 14. (b) Control parameter  $\mu = 0$ . (c) Control parameter  $\mu = 0.1$ .

## V. CONCLUSION

This paper presents the consequences of a fold catastrophe occurring in the potential of an axially symmetric system with one external parameter. The foliation of the phase space by tori is investigated for the two inequivalent canonical forms of the fold catastrophe. The first local model implies the appearance of a second sheet in the image of the energy-momentum map while the second model involves the symmetric breaking of a second sheet. The sequence of events in the second case is not the reverse seen for the first case. A family of systems with an octic potential is used to illustrate the phenomena. The proposed Hamiltonian contains the two local models. The relationship between the singularity induced by the fold catastrophe and the regularity of the joint spectrum is investigated, with an emphasis on the possible manifestation of monodromy. The displacement of an elementary cell around the singularity and the

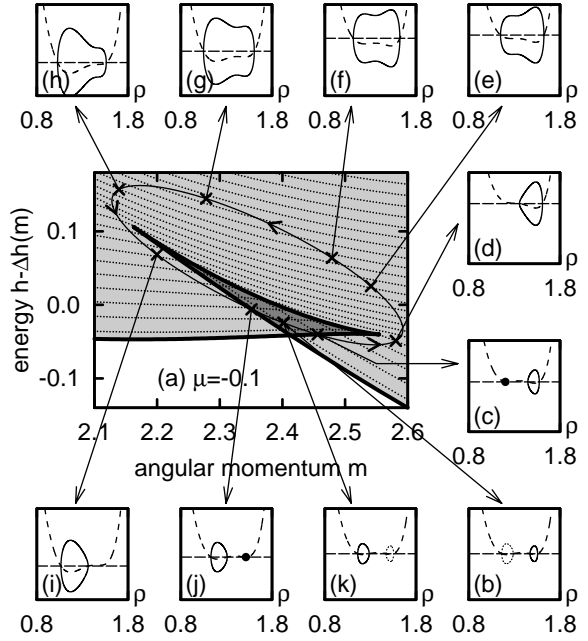


FIG. 14: (a) Enlargement of Fig. 13(a). The quantum eigenstates have been determined with the Planck constant  $\hbar = 0.005$ . The energy axis is shifted by a linear function  $\Delta h$  of the angular momentum  $m$ :  $\Delta h(m) = 1.6m - 9.06$ . (b-k) Effective potential (dashed curve), energy (horizontal dashed line) and radial momentum  $\pm p_\rho(\rho)$  (solid curves) are drawn for ten representative points in the image of the energy-momentum map. The small filled circles represent  $\pm p_\rho(\rho)$  curves reduced to one point. The evolution of a torus from panel (b) to panel (k) is seen in the continuous curves. Panels (b) and (k) have two regular tori: one is drawn as a continuous curve and the other one is drawn as a dotted curve.

absence of deformation between the initial and the final cell proves in the first case that the fold catastrophe singularity does not induce monodromy. In the second case, no closed loop around a singularity can be defined and the concept of monodromy is irrelevant. There is however a domain in the image of the energy-momentum map where the preimage of a regular point consists of two tori and it is possible to continuously transform one torus to the other one.

The concomitant existence of two sheets and monodromy in some previous studied systems is only an fortuitous accident. This paper definitively shows that the singularity induced by the fold catastrophe can be the cause of the existence of two sheets of regular values but does not introduce monodromy in the system.

The results presented in this paper illustrate one type of change with respect to the number of sheets in the image of the energy-momentum map but numerous other possibilities exist. It is known that

several sheets appear as well in the image of the energy-momentum map of the three-dimensional ellipsoid with distinct semi-axes [42] and a systematic description of the possible modifications of the number of sheets would certainly be worthwhile.

### Acknowledgments

The authors would like to thank Holger Waalkens for preliminary calculations of the clas-

sical and quantum energy momentum map for an octic potential. We also thanks Andrea Giacobbe and D. A. Sadovskii for interesting discussions.

- 
- [1] B. I. Zhilinskiĭ, Phys. Rep. **341**, 85 (2001).  
 [2] L. Michel and B. I. Zhilinskiĭ, Phys. Rep. **341**, 173 (2001).  
 [3] J. J. Duistermaat, Commun. Pure Appl. Math. **33**, 687 (1980).  
 [4] R. H. Cushman and L. M. Bates, *Global Aspects of Classical Integrable Systems* (Birkhäuser, Basel, 1997).  
 [5] R. H. Cushman, Centrum voor Wiskunde en Informatica Newsletter **1**, 4 (1983).  
 [6] M. S. Child, in *Advances in Chemical Physics, Volume 136* (Wiley, 2007), pp. 39–95.  
 [7] D. A. Sadovskii and B. I. Zhilinskiĭ, Mol. Phys. **104**, 2595 (2006).  
 [8] D. A. Sadovskii and B. I. Zhilinskiĭ, Phys. Lett. A **256**, 235 (1999).  
 [9] L. Grondin, D. A. Sadovskii, and B. I. Zhilinskiĭ, Phys. Rev. A **65**, 012105 (2001).  
 [10] R. Cushman and H. Knörrer, in *Differential Geometric Methods in Mathematical Physics* (Springer Berlin/Heidelberg, 1985), vol. 1139 of *Lecture Notes in Mathematics*, pp. 12–24.  
 [11] L. M. Bates, J. Appl. Math. Phys. (ZAMP) **42**, 837 (1991).  
 [12] M. S. Child, J. Phys. A: Math. Gen. **31**, 657 (1998).  
 [13] F. Pérez-Bernal and F. Iachello, Phys. Rev. A **77**, 032115 (2008).  
 [14] R. H. Cushman and D. A. Sadovskii, Europhys. Lett. **47**, 1 (1999).  
 [15] K. Efstathiou, R. H. Cushman, and D. A. Sadovskii, Physica D **194**, 250 (2004).  
 [16] R. H. Cushman and D. A. Sadovskii, Physica D **142**, 166 (2000).  
 [17] K. Efstathiou, D. A. Sadovskii, and B. I. Zhilinskiĭ, Proc. R. Soc. A **463**, 1771 (2007).  
 [18] H. Waalkens, H. R. Dullin, and P. H. Richter, Physica D **196**, 265 (2004).  
 [19] H. Dullin, A. Giacobbe, and R. Cushman, Physica D **190**, 15 (2004).  
 [20] A. Giacobbe, R. H. Cushman, D. A. Sadovskii, and B. I. Zhilinskiĭ, J. Math. Phys. **45**, 5076 (2004).  
 [21] R. H. Cushman, H. R. Dullin, A. Giacobbe, D. D. Holm, M. Joyeux, P. Lynch, D. A. Sadovskii, and B. I. Zhilinskiĭ, Phys. Rev. Lett. **93**, 024302 (2004).  
 [22] R. Thom, *Stabilité structurelle et morphogénèse* (Interéditions, Paris, 1972).  
 [23] V. I. Arnol'd, *Catastrophe Theory* (Springer, Berlin, 2004), 3rd ed.  
 [24] R. Gilmore, S. Kais, and R. D. Levine, Phys. Rev. A **34**, 2442 (1986).  
 [25] A. V. Bolsinov and A. T. Fomenko, *Integrable Hamiltonian Systems: Geometry, Topology, Classification* (Chapman & Hall/CRC Press, Boca Raton, Florida, 2004).  
 [26] H. Mineur, J. Math. Pures Appl. **XV**, 385 (1936).  
 [27] H. Mineur, Journal de l'Ecole Polytechnique **3**, 173 (1937).  
 [28] V. I. Arnol'd, *Mathematical Methods of Classical Mechanics* (Springer, New-York, 1989), 2nd ed.  
 [29] B. Zhilinskiĭ, Acta Appl. Math. **87**, 281 (2005).  
 [30] R. Cushman and J. J. Duistermaat, Bull. Amer. Math. Soc. **19**, 475 (1988).  
 [31] K. Efstathiou, in *Metamorphoses of Hamiltonian Systems with Symmetries* (Springer, 2005), vol. 1864 of *Lecture Notes in Mathematics*, pp. 87–111.  
 [32] M. Joyeux, D. A. Sadovskii, and J. Tennyson, Chem. Phys. Lett. **382**, 439 (2003).  
 [33] K. Efstathiou, M. Joyeux, and D. A. Sadovskii, Phys. Rev. A **69**, 032504 (2004).  
 [34] L. Michel and B. I. Zhilinskiĭ, Phys. Rep. **341**, 11 (2001).  
 [35] K. Efstathiou and D. Sadovskii, in *Geometric Mechanics and Symmetry: the Peyresq Lectures*, edited by J. Montaldi and T. Ratiu (Cambridge University Press, 2005), vol. 306 of *London Mathematical Society Lecture Notes Series*, pp. 211–301.  
 [36] M. Kastner, Rev. Mod. Phys. **80**, 167 (2008).  
 [37] R. Gilmore, *Catastrophe Theory for Scientists and Engineers* (Dover Publications, New York, 1993), unabridged Dover (1993) republication of the edition published by John Wiley & Sons, New York, 1981.  
 [38] A. Giacobbe, Regul. Chaotic Dyn. **12**, 717 (2007).  
 [39] A. Giacobbe, private communication.  
 [40] S. H. Dong, Int. J. Theor. Phys. **41**, 89 (2002).  
 [41] D. Sadovskii and B. Zhilinskiĭ, Ann. Phys. (N.-Y.) **322**, 164 (2007).  
 [42] C. M. Davison, H. R. Dullin, and A. V. Bolsinov, J. Geom. Phys. **57**, 2437 (2007).